Astron. Astrophys. 323, 541–548 (1997)

ASTRONOMY AND ASTROPHYSICS

High resolution imaging and spectroscopy of the Serpens reflection nebula (SRN). Evidence of a latitude-dependent wind⋆

Ana I. Gómez de Castro

Instituto de Astronomía y Geodesia (CSIC-UCM), Facultad de CC. Matemáticas, Universidad Complutense de Madrid (UCM), E-28040 Madrid, Spain

Received 10 April 1996 / Accepted 4 December 1996

Abstract. An optical study (high resolution images and long-slit spectra in the Hα range) of the Serpens reflection nebula (SRN) is presented. The SRN is a bipolar nebula illuminated by the low mass pre-main-sequence (PMS) star Serpens/SVS 2. The Hα profile of Serpens/SVS 2 is shown to be very broad (the width at a 10% of the peak intensity is 13.1 Å($\sim$ 600 km/s)). The profile has three emission peaks centered at -137, 5 and 100 km/s. The relative strength of the peaks varies with the slit orientation. The blue and redshifted components have similar intensities at low inclinations ($PA = -55^o$ and $PA = -30^o$) while at high inclinations the blueshifted component is weaker than the redshifted suggesting a significant contribution of absorption by low latitude outflowing gas. These profiles could be produced in a rotating, latitude dependent wind with the outflow axis parallel to the disk axis.

The nebular Hα profile is *double* peaked; it has a blue and a redshifted component at the same velocities as the star. The profile shows no significant variations along a given PA; the emission is best explained by single scattering of the stellar radiation. The absence of the 0-velocity emission component is suggestive of the presence of warm absorbing gas within a few stellar radii. There are several knots of gas and dust embedded within the north-western (NW) nebular lobe. These knots are connected by a faint emission, defining a helical path around the major axis of the nebula. This area is also characterized by an unusually large polarization that reaches a 30-40 % at 0.95 μm that is consistent with a concentration of large and reflecting dust grains that are presumably ice coated carbon grains. This region coincides with a ridge of hot (T $\simeq$ 35 K) dust detected by IRAS along the major axis of the SRN.

Key words: ISM: reflection nebulae – ISM: individual objects: Serpens Reflection Nebula – ISM: jets and outflows – stars: pre-main-sequence – stars: mass-loss

Send offprint requests to: Ana I. Gómez de Castro

⋆ Based on observations carried out at the Calar Alto and Roque de los Muchachos Observatories.

1. Introduction

The Serpens Reflection Nebula (SRN) is the most prominent object in the Serpens star forming region. It is characterized by a rather complex bipolar structure with several knots of dust and gas embedded in both nebular lobes. The north-western (NW) lobe is bright and well defined and the south-eastern (SE) is diffuse and fainter, and seems to run into the cloud. The star and the NW lobe are clearly seen in the K-band (Eiroa & Casali 1992). Optical CCD images can be found in Gómez de Castro, Eiroa & Lenzen (1988; hereafter GEL) and Hartigan & Lada (1985). Polarization maps in the optical range are also available (GEL, Warren-Smith et al. 1987, King, Scarrot & Taylor 1983).

Serpens/SVS 2 is the low mass pre-main-sequence (PMS) star that illuminates the SRN. Cohen & Kuhi 1979 (hereafter CK) assigned a spectral type M0 from the analysis of the optical spectra. The maximum of the near infrared energy distribution is at 3 μ m (Churchwell & Koorneeff 1983). Only faint and broad H_2O ice absorption is found at 3.1 μm in the line of sight to the star. No CO ice absorption at 4.67 μm has been detected (Eiroa & Hodapp 1989).

An interesting property of the Serpens molecular cloud is that nearly all the outflows (8 out of 10) within the 0.2 pc core are aligned parallel to the helical component of the local magnetic field (GEL). This includes seven reflection nebula detected at optical (GEL) or infrared wavelengths (Eiroa & Casali, 1992) and a PMS radiosource with bipolar radiolobes (Rodriguez et al 1989; Curiel et al 1993). This remarkable alignment can be naturally explained if the cloud magnetic field is strong enough to slow down the collapse perpendicularly to the field lines. In this case, the spherical symmetry is disrupted, and the protostellar cores become flattened pancakes oriented perpendicularly to the field (Mestel, 1965a,b). The magnetic field appears to play an active role in driving the radiosource outflow (see Henriksen et al 1991); in fact, non-thermal radiation has been detected from the radiolobes (Curiel et al 1993).

In this work, the SRN is studied in detail by means of high resolution imaging and long-slit spectroscopy. It will be shown that the structure and kinematics of the circumstellar Hα emitting region can be explained in terms of a latitude de-

pendent wind. The observations are described in Sect. 2. In Sect. 3 the main results from the observations are summarized. The implications for wind models are discussed in Sect. 4. A distance to Serpens of 311 $\pm$ 38 pc (de Lara et al. 1991) will be used throughout this work.

2. Observations

The inner area of the SRN is shown in Fig. 1 from the CCD images taken in 1984 with the 2.2 m telescope of the Calar Alto Observatory. The filters used were: RG780 ($\lambda_{\rm eff}$ = 8390 Å and $\Delta\lambda$ = 1900 Å at the 10 % level), Hα ($\lambda_{\rm eff}$ = 6557 Å and FWHM = 100 Å), [S II] ($\lambda_{\rm eff}$ = 6730 Å and FWHM = 95 Å), and C664 ($\lambda_{\rm eff}$ = 6640 Å and FWHM = 280 Å). The seeing was $\sim$ 1". A more detailed description of the images and their reduction is in GEL. As shown in Fig. 1 there is an elongated feature that extends westwards from Serpens/SVS 2. It is detected in narrow band images and in the continuum indicating a high content of dust. It bends northwards at 5" from the source. Further north, at 6" north west of the source, it bends back to the south-west giving an overall helical or firehose aspect to the dust lane (from now on the dust lane will be described as helical for conciseness).

Further images in the I band (filter passband from 7600 to 8800 Å) and in Hα ($\lambda_{\rm c}$ = 6564 Å and FWHM = 28 Å) were obtained in November 1992 with the 2.5 m Nordic Optical Telescope (NOT) at the Roque de los Muchachos Observatory (La Palma, Spain). The detector was a TEK CCD with 512 x 512 pixels of 27 μm. The focal reducer with the CCD provided a spatial scale of 0."1. The seeing was 0."6-0."8. The helically shaped dust lane was clearly visible in the I-band.

Five long-slit spectra of Serpens/SVS 2 were obtained in August 1989 with the Twin Spectrograph placed in the Cassegrain focus of the 3.5 m telescope of the Calar Alto Observatory (Almería, Spain). In the red channel of the spectrograph, the detector used was a GEC CCD with 580x410 pixels of 17 μm in size. The dispersion is 36 Å /mm and the spectrograms range approximately from 6500 to 6800 Å. In the blue channel, the detector was a RCA CCD with 1024x656 pixels of 15 μm in size. The dispersion is 72 Å/mm and the spectral range covered is $\sim$ 4300 – 5300 Å. The slit (2" wide and 240" length) was centered on Serpens/SVS 2 and oriented in the directions with Position Angle (P.A.) = $35^o, 0^o, -30^o, -55^o$ and -90^o. Each spectrum has an exposure time of 1 hour. The spatial scale along the slit is 0."634 pix^{-1} and the seeing was $\simeq$ 1". The spectra were reduced using the IRAF package and standard procedures. The consistency of the wavelength calibration for the various spectra was tested using sky lines. No absolute flux calibration was carried out. Significant nebular contribution has been detected along P.A. = $-30^o, -55^o$ and -90^o. Contour plots of the spectra in the Hα region are displayed in Fig. 2 for these orientations. The signal-to-noise ratio (S/N) goes below 3 at 12" from the star for $PA = -55^o$.

3. Results

3.1. The Serpens/SVS 2 spectrum

The flux distribution along the slit has a broad maximum at the position of Serpens/SVS 2. For each orientation, the stellar spectrum has been extracted from the position along the slit where the continuum reaches its peak intensity in order to minimize the nebular contribution. The maximum has been found by gaussian fitting. Only a weak continuum and the Hα line in emission, are detected in the individual spectra. The continuum slope ($\frac{\Delta F(\lambda)}{\Delta \lambda}$) and the H$\alpha$ profile depend on the slit orientation indicating that the circumstellar material is not distributed in a spherically symmetric envelope.

The spectra have been normalized to the continuum in the Hα region. The continuum level has been determined from two nearby windows at λ6545 - λ6555 and λ6570 - λ6580. A high S/N spectrum has been obtained by co-adding the 5 spectra. The [SII]$_{6731}$ line is detected at the 2σ level on the continuum; it has an equivalent width of $W_{[SII]}$ = 0.2 Å. The detection of the [OI]$_{6300}$ line ($W_{[OI]}$ = 1.9 Å) has been reported by CK. These characteristics of Serpens/SVS 2 are similar to those observed in other PMS stars that have forbidden line emission regions (FLERs). The electron density in the FLERs usually reaches 10^4 cm^{-3} and the [SII] lines are often saturated. The strongest lines in this density-temperature regime are Hα and [OI]$_{6300}$ and the ratio [OI]$_{6300}$/[SII]$_{6731}$ ranges typically between 2 and 10 (see Edwards et al 1987). The FLERs are shown to be associated with the presence of unresolved jets and they do likely trace the regions where jets form (see Gómez de Castro & Pudritz 1993, Gómez de Castro 1993).

Hα is very broad in Serpens/SVS 2: the width at a 10 % of the peak intensity is 13.1 Å($\sim$ 600 km/s). The profile has three emission peaks. The relative strength and the velocity of the three emission peaks varies with the slit orientation. A summary plot with the observed Hα profiles is shown in Fig. 3. A mean Hα profile has been obtained from all the Hα profiles corresponding to the different PAs (unless $PA = -90^o$ where a significant contribution from extended redshifted emission is observed (see below)). The mean profile is well fitted by three gaussians; a least squares criterion has been used for convergence and the Newton-Ramsey method for iteration. The resultant parameters are: Blue component (FWHM=3.9 $\pm$ 0.1 Å; Intensity=0.73 $\pm$ 0.02 and Central wavelength 6559.8 $\pm$ 0.06 Å), Central Component (FWHM=1.8 $\pm$ 0.1 Å; Intensity=0.42 $\pm$ 0.05 and Central wavelength 6562.9 $\pm$ 0.04 Å) and Red Component (FWHM=4.8 $\pm$ 0.2 Å; Intensity=0.98 $\pm$ 0.02 and Central wavelength 6565.0 $\pm$ 0.04 Å). The three peaks are centered at velocities -137 km/s, 5 km/s and 100 km/s. The profiles obtained with the slit oriented with PA = 35^o, -55^o and -30^o are fairly similar, however the profiles with $PA = -90^o$ and $PA = 0^o$ are different from the rest having weaker blue peaks. These last two orientations sample approximately the edge of the nebular lobes. The equivalent width of Hα , W(Hα), also depends on the orientation of the slit. W(Hα) has a mean value of 9.8 $\pm$ 0.8 reaching a maximum of 11.0 $\pm$ 1.0 Å at $PA = -90^o$ and a minimum of 8.8 $\pm$ 0.5 Å at $PA = 0^o$ (see Table 1). The

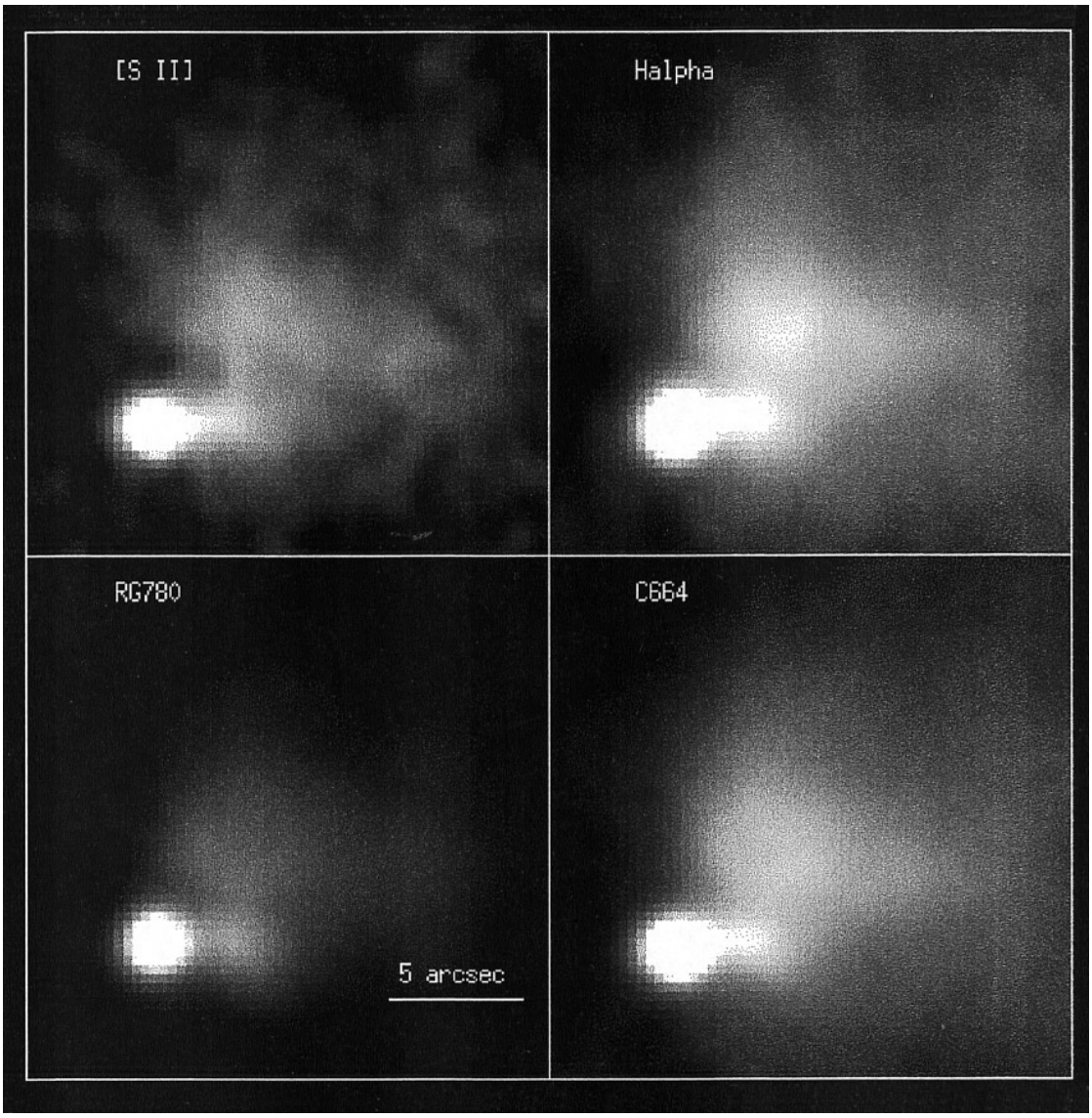

Fig. 1. CCD images of the inner 20" of the SRN's NW lobe. The images have been normalized to the same Serpens/SVS 2 flux. The constrast has been selected to describe better the nebular structure within 15 arcsec (4674 AU) of the star. There is not significant [S II] *line* emission in this band but it is the frame where the details of the nebular morphology are seen more neatly. North is at the top and East to the left.

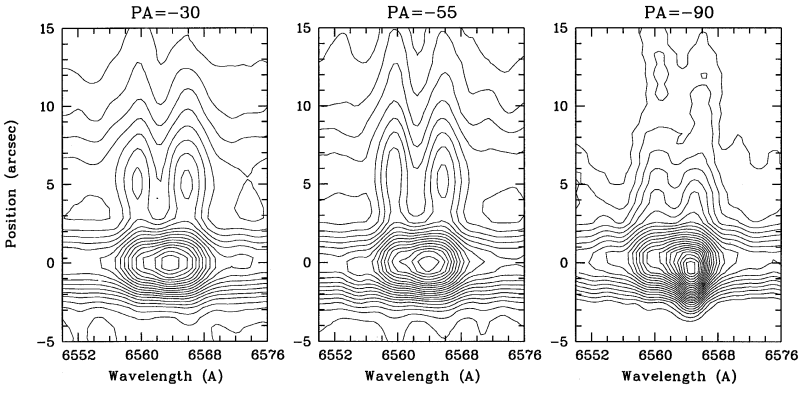

Fig. 2. Velocity-position diagrams of the SRN for the slit orientations: PA = $-30^o, -55^o$ and -90^o that sample the nebular lobes. Only the wavelengths around Hα are represented. The lowest isocontour is the 2 σ level in all the plots. The peak S/N is 81, 85 and 38 in the spectra PA = $-30^o, -55^o$ and -90^o, respectively. The isocontours are taken in 3σ units for PA = -30^o and -55^o, and in 1σ units in the spectrum with PA = -90^o. Most of the emission comes from the NW lobe (positive distances) and emission from the SE lobe is only noticeable for PA = -90^o.

Table 1. Characteristics of the stellar spectrum for the different slit orientations

P.A.	W(Hα) (Å)	$\frac{\Delta F(\lambda)}{\Delta\lambda}$ (counts/Å)
00°	8.8 ± 0.5	0.013 ± 0.005
35°	9.8 ± 0.6	-0.034 ± 0.008
-90°	11.0 ± 1.0	0.098 ± 0.004
-55°	10.1 ± 0.4	0.45 ± 0.02
-30°	9.5 ± 0.2	0.21 ± 0.01

maximum value of W(Hα) is observed at $PA = -90^o$ and it is due to the presence of an extended component eastwards of Serpens/SVS 2 (see Fig. 2). This component has the same velocity of the redshifted peak (centered at v = 89 km s^{-1}) and extends over 2."7 in this direction. The extended structure is neither observed in the continuum nor in the other velocity components of the Hα line profile indicating that the extension is not just due to the presence of a dusty condensation scattering preferentially the radiation from a particular region of the circumstellar environment.

The continuum slope varies smoothly with the PA from 0.45 at $PA = -55^o$ to the minimum, -0.034, at $PA = 35^o$, perpendicularly to the SRN major axis. The slope, $\Delta F(\lambda)/\Delta\lambda$ is given in the second column of Table 1. The errors have been calculated by least squares fitting. As the stellar radiation becomes bluer when scattered, and redder when extincted by a dusty medium, the observed trend points out that the relative mixing of scattered and directly transmitted stellar radiation changes while turning the 2" wide slit. Therefore, the circumstellar dust is concentrated in a flattened structure that is oriented close to PA= 35°, in excellent agreement with previous polarization observations (GEL).

3.2. The reflection nebula

3.2.1. The nebular Hα line

The nebular lobes are sampled by the spectra at $PA = -30°, -55°, -90°$ (see Fig. 2). The nebular spectra are dominated by the Hα line and a faint continuum. The Hα profile is *double* peaked; it has a blue and a redshifted component at the same velocities as the star. The profile does not show significant variations along a given PA.

The high polarization of the SRN (GEL) and its centrosymmetric pattern indicates that the nebula is illuminated by *single scattering* of the stellar photons. The radiation from the SRN is dominated by scattered light from Serpens/SVS 2. The most noticeable difference between the stellar and nebular profiles is the *absence of the 0-velocity emission component in the nebular profile*. This is most likely due to the presence of warm absorbing gas between the star and the nebula. The absorbing gas is at rest with respect to the star and has a velocity dispersion of 153 km s^{-1}. This velocity dispersion is much larger than that expected for a cold molecular cloud or the interstellar medium (typically $\sim$ 7 km s^{-1}); moreover it is highly suprathermal. This indicates that it is produced by warm and *turbulent* gas. Neither the velocity nor the velocity dispersion of the absorption component change with the distance to the star or the position angle. Moreover, since the line is rapidly saturated, most of the absorbing material is likely concentrated within 2"-3" around Serpens/SVS 2 and presumably closer (within few stellar radii from the star) where the hydrogen is excited to the level n=2.

3.2.2. Physical properties of the nebular dust

A bipolar CO outflow has been detected and mapped in Serpens (Bally & Lada, 1983) although the spatial resolution is not good enough to study the individual contribution of Serpens/SVS 2 to it. The outflow is centered in the SRN. The full width of the line in OH and CO is 28 km s^{-1}. Also a ridge of hot (T $\simeq$ 35 K) dust has been detected in the IRAS 50-100 μm colour map extending $\sim 5'$ from the southeast to the northwest along the major axis of Serpens/SVS 2. Zhang et al 1988 have shown that shocks, presumably related with the interaction between Serpens/SVS 2 outflow and the environmental gas, are required to heat the dust at such large distances from Serpens/SVS 2.

The properties of the dust in the outflow may be different from the rest of the nebula. This can be checked in the C664-I colour image (see Fig. 4). The NW lobe is typically 1 mag. bluer than Serpens/SVS 2 ; the helical dust lane is readily recognized on top of it (since it is only 0.3 mag bluer than Serpens/SVS 2). There is also a large region along the major axis of the SRN where the emission is 0.4-0.2 mag. redder than the nebular background. The helical dust lane and this area are also characterized by an unsually large polarization at 0.95 μm that reaches a 30-40 % (GEL), indicating that there is a concentration of *large ($> 0.95\mu m$) and reflecting dust grains* that are presumably silicates or ice coated carbon grains. As the 3.1 μm ice band has been detected towards several objects in Serpens, including Serpens/SVS 2 (Eiroa and Hodapp, 1989; Chiar et al 1994) this is probably a more consistent explanation. The observed value of R=4 for the Serpens molecular cloud (Chavarría et al, 1987) also indicates that the grains are larger than the interstellar ones.

The slope of the nebular continuum varies at certain locations in the nebula. For instance, along $PA = -55^o$ the scattered spectrum is bluer than the stellar one with a typical flat slope: $\frac{\Delta F(\lambda)}{\Delta\lambda} \simeq 0.02 \pm 0.01$ counts/Å. However at distances between 4."5 and 6."4, coinciding with the location of the helical dust lane, the spectrum is significantly redder than in the rest of the nebula with $\frac{\Delta F(\lambda)}{\Delta\lambda} \simeq 0.11 \pm 0.01$ counts/Å. The nebular spectra taken closer or farther from the star than the dust lane are similar indicating that it only covers a small solid angle of the stellar light beam. In principle, the variation of the continuum slope could also be due to dust luminescence. This is observed in some reflection nebulae like NGC 7023 producing an extended red emission (ERE) feature that peaks near 6800 Å. ERE have been proposed to be due to photoluminescence of hydrogenated carbon (Witt, 1988, Witt and Schild, 1988; Watanabe, Hasegawa and Kurata, 1982). The likely excitation source for the ERE are mid-UV photons from the illuminating stars (Witt and Schild,

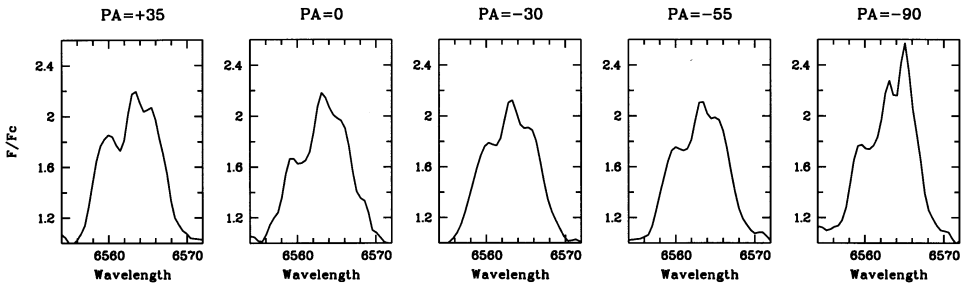

Fig. 3. The stellar Hα profile normalized to the continuum, for all the slit orientations.

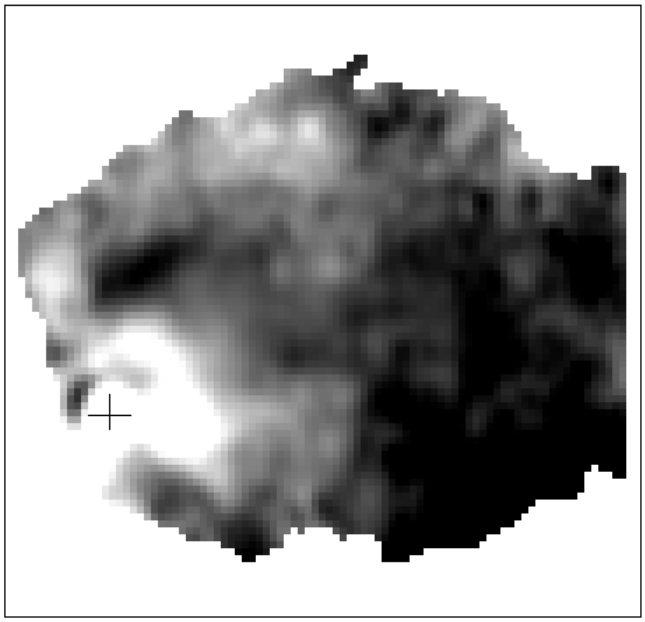

Fig. 4. C664-I colour plot of the SRN. North is up and east to the left. The location of Serpens/SVS 2 is marked with a cross; the position of the condensation C1 is also indicated to point out the scale. The small region, north of Serpens/SVS 2, that is redder than the rest of the nebula is illuminated in part by the nearby PMS star, GEL 8 (see GEL).

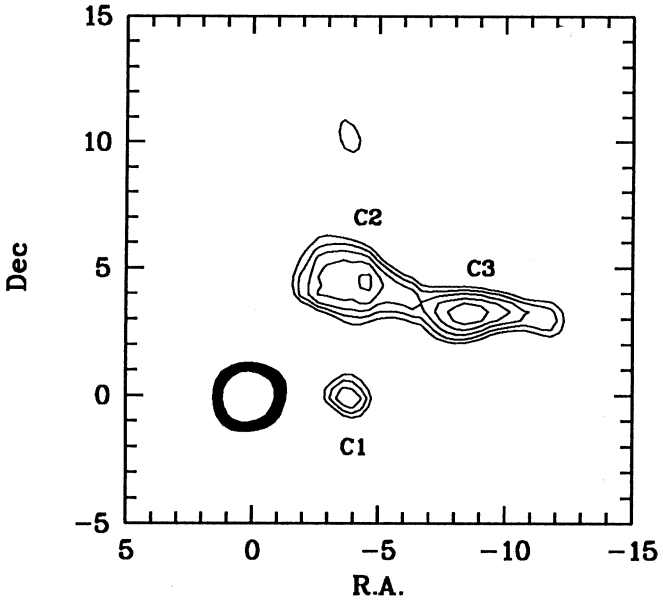

Fig. 5. Small scale structure of the SRN revealed after applying a laplacian adaptative filtering to the Hα image. North is up and East to the right. The distance between two large tickmarks is 5" and between 2 small tickmarks 1". Serpens/SVS 2 is at (0,0).

1985), normally A stars. Note however, that Serpens/SVS 2 is an M type star.

A laplacian adaptative filtering has been applied to the Hα image to unveil the small scale structure embedded in the large conical lobe. Adaptative filtering has been developed by Lorenz et al 1993; the reader is referred to this publication for a detailed description of the technique. After filtering only the star and several knots associated with the "helical" dust lane are left (see Fig. 5). The coordinates of the knots are given in Table 2.

Table 2. Coordinates of the condensations within Serpens/SVS 2 NW lobe

Iden.	α(1950)			δ(1950			r	PA
	(h)	(m)	(s)	(°)	(')	(")	"	°
C1	18	27	24.3	1	12	40.9	3.3	-88
C2			24.2			45.0	6.1	-50
C3			24.0			44.6	8.2	-65

3.3. Detection of a Herbig-Haro nebulosity

A shock excited nebulosity has been detected in the spectra 88" eastwards of Serpens/SVS 2 . The HH object emits in the Hα, [S II] and [N II] lines, and is at rest with respect to the star. The nebulosity extends along 4.4 arcsec or 1370 AU in the east-west direction and has some structure in the position-velocity diagram. The electronic density inferred from the [S II] lines ratio is 1.8×10^2 cm^{-3}. The ratio of Hα to [N II] and [S II] is 1.1 and 0.4 respectively, indicating that the excitation is low and similar to that observed in optical jets. Reipurth & Eiroa 1992 detected several HH objects in the cloud but far from this region.

4. Discussion

4.1. Variability

There are few PMS objects driving bipolar outflows that allow detailed optical studies (see Staude & Elsaesser 1993 for a recent review). At first glance, the phenomenology observed in the SRN resembles that of R Mon. There are however noteworthy differences. R Mon shows a low excitation emission line spectrum superposed on the Balmer series lines seen in absorption. The cometary nebula associated with R Mon, NGC 2261, shows a variation with the velocity of the reflected absorption spectrum as a function of distance from R Mon (Stockton et al 1975). The emission lines in the reflected spectrum show no significant variations and henceforth, differential motions within the nebula cannot be responsible for the absorption line variations that are attributed to variations in the absorption shell around R Mon. In Serpens/SVS 2 the absorption component is not variable in velocity but it is at rest with respect to the star. No variations have been detected in the morphology of the nebula or in the distribution of the dust condensations. Comparison between the sparse CCD images of the nebula obtained during the last years (King et al 83, Hartigan & Lada 1985, Warren-Smith et al 87, GEL, NOT images) do not show hints of variations in the nebular morphology.

The equivalent width of Hα measured in this work is larger than the obtained by CK: W(Hα) = 5.5 Å. This difference could be due to the larger integration area they used (2."7x4" instead of 1"x2" in this work) that dilutes the Hα contribution. Another possibility is that Serpens/SVS 2 is variable. In principle, this could also explain the differences between the stellar and the nebular Hα profile. Variations in time scales between 1.8 and 14 days can be tracked in the nebular spectrum since the dominant contribution to the SRN spectrum is the scattered light from the star. The limits are set by the light travel time to cross 1" (the spatial resolution limit set by the seeing) and to cross the extent of the nebula in the long-slit spectra ($\sim$ 8"),respectively. These variations can be best sorted out by plotting Hα normalized to the continuum in all the nebular positions. The Hα photons are *scattered* by the dust grains in the same manner as the nearby continuum, henceforth the Hα profile normalized to the continuum should be the same all over the nebula provided that there is no absorbing or emitting gas. In the case of pure scattering (no nebular emission or absorption) and if Serpens/SVS 2 is not variable the contours in Fig. 6 should be parallel straight lines running along the slit direction and reproducing the intensity levels of the illuminating stellar Hα emission. Only at distances comparable to the size of the dust pancake this interpretation is not valid. Note that in such a dense environment geometric effects and multiple scattering are relevant and moreover, the mean illuminating Hα profile is a mixture of the profiles displayed in Fig. 3. The contours in Fig. 6 reproduce similar intensity levels for the blue and red components in the star and nebula along $PA = -30^o$ and -55^o; the flux of the 0-velocity component drops rapidly in the nebula and remains rather constant. Therefore it is unlikely that Serpens/SVS 2 was varying on scales between 1.8 and 14 days before the long-slit spectra were obtained. However, *a monitoring of the SRN is required to rule out definitely that Serpens/SVS 2 is variable*. Only variations in the line fluxes > 10 % could be detected from these data with this method since the S/N of the position-velocity plots in Fig.6 is typically 10 (for P.A. = -30^o and -55^o).

4.2. A latitude-dependent wind from Serpens/SVS 2

Highly collimated dense outflows are the first signature of star formation. They are somehow linked to the release of angular momentum and gravitational energy required to form a star. In this respect it is expected that the high mass-loss rates observed in the T Tauri Stars (TTS) are driven by accretion powered winds either from the boundary layer between the star and the disk (Pringle 1989) or from the inner part of the accretion disk itself (see Pudritz et al 1991 for a review). These winds are not spherically symmetric but latitude-dependent and they are often modelled as flowing along a cone-like geometry; they are assumed to depart from the disk plane and to occupy a region between two conical surfaces of angles $\theta 1$ and $\theta 2$, where θ is the angle between the disk axis and the conical surface. For such outflows, it is expected that the observed line profile depends on the angle between the line of sight and the accretion disk axis. The interpretation of the Hα and forbidden lines profiles of the TTS is usually made within this framework (Edwards et al 1987, Calvet et al 1992; Gómez de Castro & Pudritz 1993). The conical reflection nebula illuminated by Serpens/SVS 2 provides the unique opportunity to observe the wind emission from various lines of sight. The profiles observed are indeed suggestive of a latitude dependent wind; the blue and redshifted components have similar intensities at low inclinations ($PA = -55^o$ and $PA = -30^o$), while at high inclinations the blueshifted component is weaker than the redshifted one suggesting a significant contribution of absorption by low-latitude outflowing gas. The only exception to this trend corresponds to PA=35^o where the blue component is as bright as along $PA = -55^o$. This is due to the dominant contribution of "on-axis" photons to the radiation scattered by the circumstellar dust pancake (see also Sect. 3.1).

If winds are driven mainly by accretion energy, then the wind must come from a radius of sufficient depth in the gravitational potential well so that enough energy per unit mass is available. In practice, this means that the wind radius must be around $\sim 10 - 100$ the stellar radius (Pringle 1989). Calvet et al (1992) computed the expected Balmer line profiles for inner disk winds. They show that, in general, the strength of the blueshifted emission component decreases as the inclination increases due to absorption by the outflowing gas. The effect is much more significant for rotating winds (as the disk winds) than from monotonically expanding winds with large turbulent velocities. Also, they found a strong relation between the strength of the Balmer lines and the opening angle of the outflow for monotonically expanding winds; typically the Hα line (normalized to the continuum) is 5 times stronger in winds confined within conical surfaces with large opening angles (e.g. $\theta \epsilon (50^o, 80^o)$) than in winds confined within narrow conical surfaces (e.g. $\theta \epsilon (10^o, 40^o)$). In this view, the small equivalent

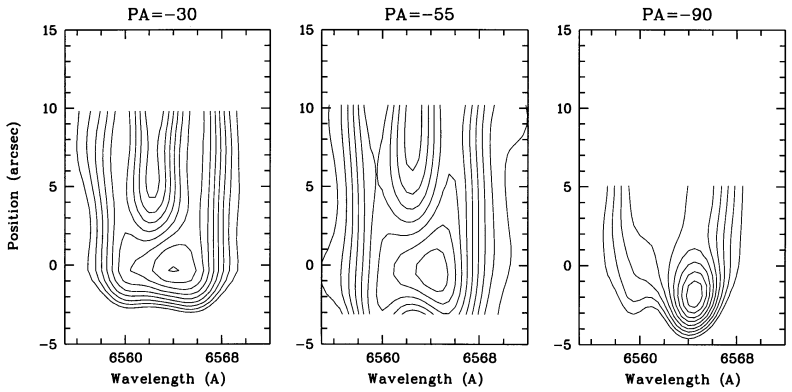

Fig. 6. Hα emission from the SRN along $PA = -30^o, -55^o$ and -90^o. The contours plot is normalized to the continuum; levels are 1,2,3,4...σ for $PA = -30^o$ and 1,3,5,7... σ for $PA = -55^o$ and -90^o. At distances $\geq$ 10" from the star the continuum signal fades away rapidly and henceforth the Hα intensity normalized to the continuum rises artificially. Only the inner 10" are reliable to study the line at $PA = -30^\circ$ and -55°, and the inner 5" at $PA = -90^o$.

width of the Hα line in Serpens/SVS 2 suggests that the outflow opening angle is small. On the contrary, a large opening angle of the conical surface could better explain why the latitude dependent effects are significant in Serpens/SVS 2 for so large inclinations ($PA = 0^o$ or $PA = -90^o$). The Hα equivalent width expected for the rotating wind model is smaller than the expected for conical outflows, and it seems somewhat closer to the observations. Yet there are significant differences between the computed profiles and the observed in Serpens/SVS 2.

To summarize, the Hα profiles can be explained as produced in a rotating, latitude dependent wind with the outflow axis parallel to the disk axis as expected for accretion driven disk (or boundary layer) winds. Since driving by thermal pressure in TTS outflows is unlikely (Pudritz & Norman 1986, Shu et al 1988) magnetic forces could be involved in the driving mechanism. It is worth mentioning that magnetic fields seem to have played a significant role in the formation of the Serpens/SVS 2 (GEL). Note that the collapse seems to have been sub-alfvénic since the disk axis is aligned with the direction of the molecular cloud magnetic field (Casali, private communication).

5. Conclusions

The optical study of the Serpens/SVS 2 and the reflection nebula illuminated by it shows that:

- The Hα profile of Serpens/SVS 2 is very broad (the width at a 10% of the peak intensity is 13.1 Å($\sim$ 600 km/s)). The profile has three emission peaks centered at -137, 5 and 100 km/s. The relative strength of the peaks varies with the slit orientation. The blue and redshifted components have similar intensities at low inclinations ($PA = -55^o$ and $PA = -30^o$) while at large inclinations the blueshifted component is weaker than the redshifted suggesting a significant contribution of absorption by low latitude outflowing gas. It is shown that the observed trend can be *qualitatively* explained within the context of latitude dependent winds.
- There is a helical dust lane embedded in the northwestern lobe. Large and highly refractory grains have been detected in the helical dust lane and along the major axis of the nebula. They are presumably ice coated carbon grains. The scattered spectrum is redder at these locations than in the rest of the nebula.
- Warm gas absorbing Hα photons has been detected around the star. The line width is 153 km s $^{-1}$; this value is highly suprathermal indicating that the absorption occurs in a turbulent environment. Most of the absorption is expected to be produced within few stellar radii where there is enough hot gas to populate the n=2 level of hydrogen.
- Our observations strongly suggest that Serpens/SVS 2 was not variable on time scales between 1.8 and 14 days before the long-slit spectra were obtained, at flux levels $\leq$ 10 %. However a continuous monitoring of the SRN is strongly required to rule out that Serpens/SVS 2 and the SRN are not variable.

Acknowledgements. It is a pleasure to thank A. Jones and J.L. Greenstein for our conversations on dust properties. I also thank Drs. G.M. Richter and G. Longo for their help with applying adaptative filtering to the CCD images and Drs. R. Mundt and M. Fridlund for their comments on the manuscript. Most of this work was carried out while I was enjoying a "re-entry" fellowship from the Ministerio de Educación y Ciencia (MEC) of Spain in the ESA IUE Observatory in VILSPA (Madrid). I want to thank the staff at VILSPA and the MEC for their support. I thank the staff of the Calar Alto Observatory and of the NOT for their assistence during the observations. This work was partially supported by the DGCYT grant PB93-0461

References

Bally, J., Lada, C.J. 1983, ApJ, 265, 824
Bohlin, R.C., Savage, B.D., Drake, J.K. 1978, ApJ, 224, 132
Calvet, N., Hartmann, L., Hewett, R., 1992, Ap J, 386,229
Chavarría-k, C., Ocegueda, J., de Lara, E., Finkenzeller, U., Mendoza, E. 1987, IAU Symp. 122, Reidel, Dordrecht, 97
Chiar, J.E., Adamson, A.J., Kerr, T.H., Whittet, D.C.B. 1994, Ap J, 426, 240
Churchwell, E., Koornneef, J., 1986, ApJ, 300, 729
Cohen, M., Kuhi, L.V. 1979, ApJS, 41, 743
Curiel, S., Rodriguez, L.F., Moran, J.M., Canto, J. 1993, ApJ, 415, 191
de Lara, E., Chavarría-K, C., López-Medina, G., 1991; A & A, 243, 139
Edwards, S., Cabrit, S., Strom, S.E., Heyer, I., Strom, K.M., Anderson, E., 1987, ApJ, 321, 473
Eiroa,C., Hodapp, K.-W. 1989, A & A, 210, 345
Eiroa,C., Casali, M.M. 1992, A & A, 262, 468
Gómez de Castro, A.I. 1989, A& A, IAU Symp. 140, Kluwer, Dordrecht, 318

Gómez de Castro, A.I., Eiroa, C., Lenzen, R. 1988, A& A, 201,299 (GEL)
Gómez de Castro, A.I., Pudritz, R.E., 1993, ApJ, 400, 748
Gómez de Castro, A.I., 1993, ApJ, 412, L43
Hartigan, P., Lada, C.J. 1985, ApJS, 59, 383
Henriksen, R.N., Ptuskin , V.S. , Mirabel, I.F. 1991, A&A, 248,221
Kaplan, S.A., Pilkener, S.B. 1970, The Interstellar Medium, ed. Harvard Univ. Press, Cambridge, Massachusetts, 187
King, D.J., Scarrott, S.M., Taylor, K.N.R. 1983, MNRAS, 202, 1087
Lorenz, H., Richter, G.M., Capaccioli, M., Longo, G., 1993, A& A, 277, 321
Mestel, L. 1965a, Quart. JRAS, 6, 161
Mestel, L. 1965b, Quart. JRAS, 6, 265
Pringle, J.E., 1989, MNRAS, 236, 107
Pudritz, R.E., Norman, C.A. 1986, ApJ, 301, 571
Pudritz, R.E., Pelletier, G., Gómez de Castro, A.I. 1991; NATO ASI on The physics of star formation and early stellar evolution, eds. Lada, C.J. and Kylafis, N.D. (Kluwer), 539
Reipurth, B., Eiroa, C. 1992, A & A, 256 , L1
Rodriguez, L.F., Curiel, S., Moran, J.M., Mirabel, I.F., Roth, M.,Garay, G. 1989, ApJ, 346, L85
Shu, F.H., Lizano, S., Ruden, S.P., Najita, J., 1988, ApJ, 328, L19
Staude, H.J., Elsaesser, H., 1993, A & AR, 5, 167
Stockton, A.M., Chesley, D., Chesley, S., 1975, ApJ, 199,406
Ungerechts, H., Gusten, R. 1984, A & A, 131, 177
Warren-Smith, R.F., Draper, P.W., Scarrot, S.M. 1987, MNRAS, 227,749
Watanabe, I., Hasegawa, S., Kurata, Y. 1982, Japanase J. Appl. Phys., 21, 856
Witt, A.N. 1988, Dust in the Universe, eds. M.E, Bailey and D.A.Williams, Cambridge Univ. Press, 1
Whittet, D.C.B. 1992, Dust in the galactic environment, The Graduate Series in Astronomy, eds. R.J. Taylor and R.E. White, Institute of Physics Publishing, London, 69
Witt, A.N., Schild, R.E. 1988, ApJ, 325, 837
Zhang, C.Y., Laureijs, R.J., Clark, F.O. 1988,, A & Ap, 196,236

This article was processed by the author using Springer-Verlag LaTeX A&A style file *L-AA* version 3.